Fluorescent Probe Hot Paper

How to cite:
International Edition: doi.org/10.1002/anie.202202961
German Edition: doi.org/10.1002/ange.202202961

An Acid-Regulated Self-Blinking Fluorescent Probe for Resolving Whole-Cell Lysosomes with Long-Term Nanoscopy

*Qinglong Qiao, Wenjuan Liu, Jie Chen, Xia Wu, Fei Deng, Xiangning Fang, Ning Xu, Wei Zhou, Shaowei Wu, Wenting Yin, Xiaogang Liu, and Zhaochao Xu**

Abstract: Long-term super-resolution imaging appears to be increasingly important for unraveling organelle dynamics at the nanoscale, but is challenging due to the need for highly photostable and environment-sensitive fluorescent probes. Here, we report a self-blinking fluorophore that achieved 12 nm spatial resolution and 20 ms time resolution under acidic lysosomal conditions. This fluorophore was successfully applied in super-resolution imaging of lysosomal dynamics over 40 min. The pH dependence of the dye during blinking made the fluorophore sensitive to lysosomal pH. This probe enables simultaneous dynamic and pH recognition of all lysosomes in the entire cell at the single-lysosome-resolved level, which allowed us to resolve whole-cell lysosome subpopulations based on lysosomal distribution, size, and luminal pH. We also observed a variety of lysosome movement trajectories and different types of interactions modes between lysosomes.

Lysosomes are multifuctional organelles with roles in degrading macromolecules, mediating cell metabolism and cellular signalling.[1] Growing evidence suggests that each lysosome with different motion trail destine and chemical composition at a different location has specific functions.[2] In addition, the whole-cell scale spatial organization of lysosomes can be regulated at the systems level to function across the entire intracellular space,[3] such as the formation of lysosomal clusters. Deciphering the spatial distribution, chemical composition, and dynamics of whole-cell lysosomes could enable in-depth understanding and even discover the multifunctionality of lysosomes. This has spurred the development of imaging techniques to uncover lysosome subpopulations based on their movement,[4] morphology,[5] spatial distribution,[3] and proton/chloride ion concentrations.[6] However, the relationship between the location, chemical composition, and dynamic behaviors of lysosomes remains ambiguous.[2] The heterogeneity of intracellular lysosomes and the uncertainty and unpredictability of their dynamic behaviors further exacerbate the difficulty of observing and resolving intracellular lysosomes.[7] Fortunately, in recent years, there have been rapid improvements in super-resolution imaging techniques that can image individual lysosomes at the nanoscale regime.[8] However, as these fluorophores lack sufficient photo-stability for long-term nanoscopy, and these probes mainly function as lysosome tracking without sensitivity to the luminal pH (4.5–5), the ability to resolve whole-cell lysosomal dynamics and chemical compositions at the individual lysosome level remains a challenge.

The first self-blinking HMSiR dye was pioneered by Urano et al. and has been successfully applied in single-molecule localization microscopy (SMLM).[9] The rapid switching between the non-fluorescent spirocyclic rhodamine form and the fluorescent zwitterionic form allowed for multiple positioning of the dye molecules at different regions of the cell, enabling dynamic super-resolution imaging of living cells. Most importantly, high-density HMSiR probes positioned on the lipid membrane achieved long-term super-resolution imaging.[10] The reason for such excellent photostability is likely ascribed to recently reported buffer strategies.[7] For HMSiR and its subsequent self-blinking derivatives, the chemical modification of the xanthene scaffold such that pK_{cycl} is less than 6, can ensure that a small number of dyes are in the fluorescent state at physiological pH 7.4, while most dyes are in the non-emissive closed form (as shown in Scheme 1a).[11] To obtain self-blinking dyes under lysosomal pH, it is necessary to further reduce pK_{cycl} to about 3, to ensure that only a small number of dyes are in the fluorescent zwitterionic form at pH 4.5–5 (Scheme 1a).

In this work, we introduced an *o*-methylpyridine moiety into the spirolactam scaffold (Scheme 1b) and obtained the dye **LysoSR-549** which had a pK_{cycl} of 3.2, and is suitable for SMLM at lysosomal pH (Figure 1a, S1). **LysoSR-549** can resolve the number, size, distribution, and dynamics of lysosomes in the whole cell with the resolution of individual lysosomes, and also simultaneously probe the pH of these lysosome subpopulations and even the luminal pH of individual lysosomes.

Pyridine is in a planar structure with isoindolin-1-one, and the pyridine N is in a reverse position with the carbonyl group (as shown in the crystal structure in Scheme 1b, S2).

[*] Dr. Q. Qiao, W. Liu, J. Chen, Dr. F. Deng, X. Fang, N. Xu, W. Zhou, S. Wu, Dr. W. Yin, Prof. Dr. Z. Xu
CAS Key Laboratory of Separation Science for Analytical Chemistry, Dalian Institute of Chemical Physics, Chinese Academy of Sciences
457 Zhongshan Road, Dalian 116023 (China)
W. Liu, J. Chen, X. Fang, S. Wu, Prof. Dr. Z. Xu
University of Chinese Academy of Sciences
Beijing 100049 (China)
E-mail: zcxu@dicp.ac.cn
X. Wu, Prof. Dr. X. Liu
Singapore University of Technology and Design
8 Somapah Road, Singapore 487372 (Singapore)

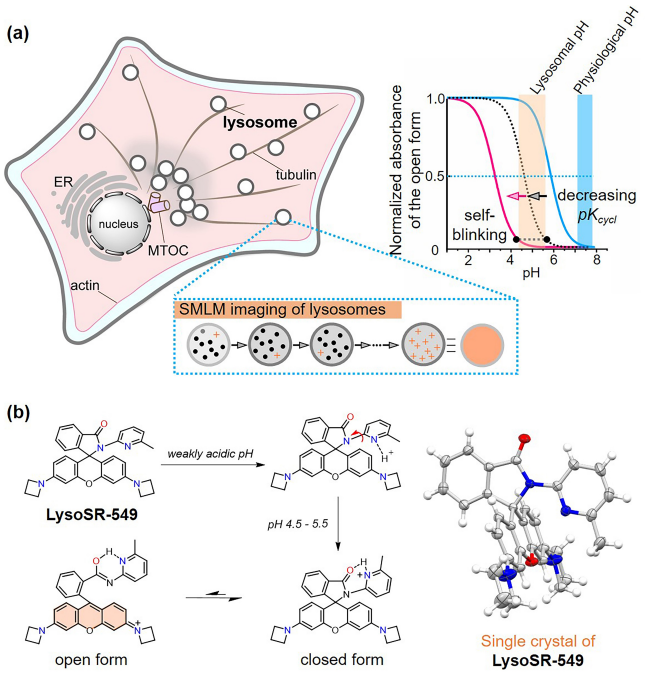

Scheme 1. a) Intracellular distribution of lysosomes and SMLM imaging of lysosomes. b) Mechanism of spontaneously blinking in lysosomal pH. Illustration: Single crystal of **LysoSR-549**.

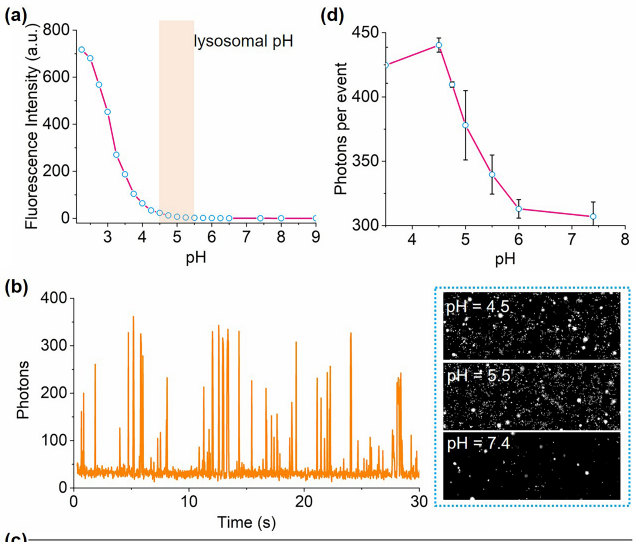

(c)

pH	photons per event	location accurcy (nm)	total moecules ($\times 10^4$)	percent of ON molecules
3.50	425 ± 14	31.4 ± 0.40	2.93 ± 0.12	0.2687
4.50	440 ± 6	30.9 ± 0.44	2.28 ± 0.05	0.0136
5.00	378 ± 27	31.4 ± 0.68	1.99 ± 0.22	0.0042
5.50	340 ± 15	34.6 ± 0.26	1.71 ± 0.14	0.0014
6.00	313 ± 7	36.7 ± 0.78	1.61 ± 0.12	0.0007
7.40	307 ± 11	38.6 ± 1.46	-	0.0002

Figure 1. a) Fluorescence intensity of **LysoSR-549** at 583 nm as a function of pH in aqueous solution. b) Representative single-molecule fluorescence traces of **LysoSR-549**. Inserted patterns: SMLM imaging of **LysoSR-549** on hydroxylated glass sheet at different pH. c) Summary of single-molecule characteristics of **LysoSR-549**. d) Photons per event as a function of pH.

The basicity of pyridine is larger than that of carbonyl group. In **LysoSR-549**, under weakly acidic conditions, the protons are preferentially bound to the basic N of pyridine and away from the carbonyl group (Scheme 1b). As the acidity increases, the pyridine ring can rotate such that the carbonyl group can also form a hydrogen bond with the proton, in a bifurcated manner. This conformational change can enable a small number of dyes, at the range of pH 4.5–5.5, to undergo a spirolactam ring-opening reaction to form the fluorescent zwitterion. Subsequently, a nucleophilic addition reaction between the amide N with the meso-C of xanthene quickly restores the non-fluorescent spirolactam, thus completing one blinking cycle.

Analysis of the fluorescence intensity of **LysoSR-549** at varying pH conditions revealed that the proportion of fluorescent zwitterion at lysosomal pH was small to be suitable for SMLM (Figure 1a). It also showed that under physiological pH 7.4, the dyes were basically in non-fluorescent spirolactam form, thus ensuring the fluorogenicity of lysosome staining. The selectivity of **LysoSR-549** for lysosomes was further confirmed by colocalization with lysosomal membrane protein Lamp1 encoded with GFP in living cells (Figure S3). The probe was also biocompatible and did not interfere with intracellular metal ions (Figure S4, S5).

The probes, distributed on a hydroxylated glass sheet, could undergo multiple cycles of fluorescence ON/OFF switching in the range of pH 4.5–5.5 (Figure 1b), exhibiting excellent blinking properties for single molecule localization. Moreover, the increase in acidity stabilizes the fluorescent form which in turn increases the number of blinking molecules and the number of photons per event (Figure 1c, S6–S13). Between pH 4.5–6, there is excellent sensitivity and linearity between the photophysical properties of the single molecule towards proton concentration (Figure 1d). In this way, the pH in a single lysosome can be probed according to the number of photons observed in SMLM.

Spatiotemporal super-resolution imaging of lysosomes in living cells was then successfully achieved using SMLM (Movie 1). The best spatial resolution reached 12 nm, with a time resolution of 20 ms (Figure 2). Changing probe concentrations or excitation laser intensities had little effect on the SMLM imaging (Figures S14–S23). For example, a 20 nm localization accuracy can be obtained even with a 60 $W\,cm^{-2}$ excitation laser (Figure S15). The proportion of open-form of **LysoSR-549** reached the maximum value at pH 2.25, but nearly 60 % of the probes remained in the non-fluorescent closed-ring form (Table S1, Figure 1c). This proves that **LysoSR-549** has a buffering capacity, that is, the closed-ring probes in the lysosome will be converted into the opened-ring form to replace the photobleached ones, thereby ensuring prolonged (up to 40 min) photostability for super-resolution imaging (Figure S24, S25).

Lysosomal movements within the whole cell were then resolved to be dependent on location and pH and can be divided into heterogeneous subpopulations. The longest observed movement trajectory can reach 50 μm (Figure 3), and the fastest movement speed can reach 0.31 $\mu m\,s^{-1}$ (Figure 2). Figure 2a–k and Movie 2 show the movement

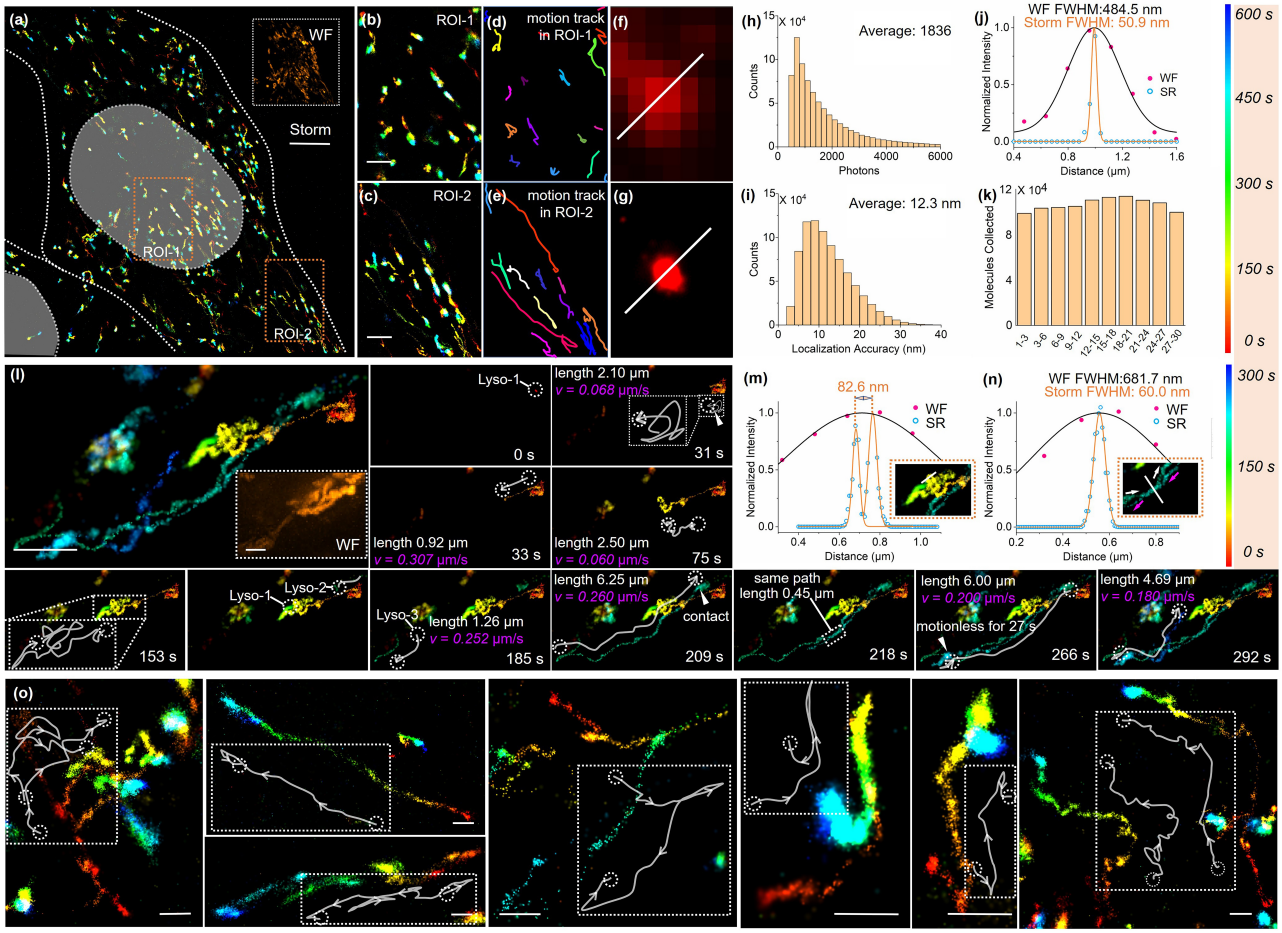

Figure 2. a) Long-term SMLM imaging of whole-cell lysosomes with **LysoSR-549** in live HeLa cells. Scale bar: 5 μm. Inset: Wide-field imaging. b) SMLM imaging of perinuclear lysosomes (ROI-1) and c) peripheral lysosomes (ROI-2), Scale bar: 1 μm. d) Movement route of perinuclear lysosomes and e) peripheral lysosomes. f) SMLM imaging and g) wide-field (WF) imaging of lysosomes in (a). h) Histograms of photons per single molecule per frame and j) localization accuracy. i) Intensity distributions across the white lines in (f) and (g). k) Variation curve of molecule detected in ROI-1 during imaging. Every 3000 frames were reconstructed for analysis of molecules detected. l) Long-term SMLM imaging of the region of interest and overlaid time-lapse images of lysosomes. Scale bar: 1 μm. m, n) Intensity distributions across movement path to demonstrate the resolution at the nanoscale and complexity of lysosomal movement which can't be distinguished through WF. o) Representative lysosomal movements. Scale bar: 0.5 μm. The cutoff value was 500 photons.

trajectories of lysosomes in one whole cell within 10 minutes, with red denoting time zero and blue denoting the end of the recording. Due to the durable chemoswitching of **LysoSR-549**, more than 120000 frames could be continuously recorded to panoramically observe lysosomes in living cells (Figure S24). The number of blinking molecules detected remained unchanged during every 30000 frames (Figure 2K, S26). The time-colored SMLM images (Figure 2a, reconstructed from 30000 frames) show the dynamics of every lysosome including motion trail, speed of movement, lysosome-lysosome contact, and distribution, with an average of 1836 photons detected and a high localization precision of 12.3 nm (Figure 2h–i). The lysosomes were about ≈50.9 nm in width under super-resolution imaging, whereas it was shown to be about 484.5 nm using WF (Figure 2j). Through the long-term SMLM, we noticed the heterogeneous moveability of lysosomes at different positions. From Movie 2, the lysosomes were observed to form multiple clusters in the cell, and the number of clusters distributed around the nucleus and along the cell periphery was quite similar. Taking the ROI-1 area as the representative region near the nucleus and ROI-2 as the representative region of the cell periphery, it was observed that the lysosomes in the ROI-1 area had relatively good dispersion, short movement trajectories, and little difference between them. However, the lysosomes in the ROI-2 region were relatively more concentrated, with longer movement trajectories and large differences between them. The speed and direction of the lysosome's entire trajectory are constantly fluctuating, and the trajectories can be split into multiple stages. Lysosome 1 (Lyso-1), as shown in Figure 1i and Movie 3, generally moved at a slow speed in an undulating manner from 0 to 31 seconds; between 31 and 33 seconds, it traveled 0.92 μm in a straight line at an extremely fast speed. Immediately after a sudden pause, it moved 2.5 μm in one direction at a very slow speed until 75 seconds; then it

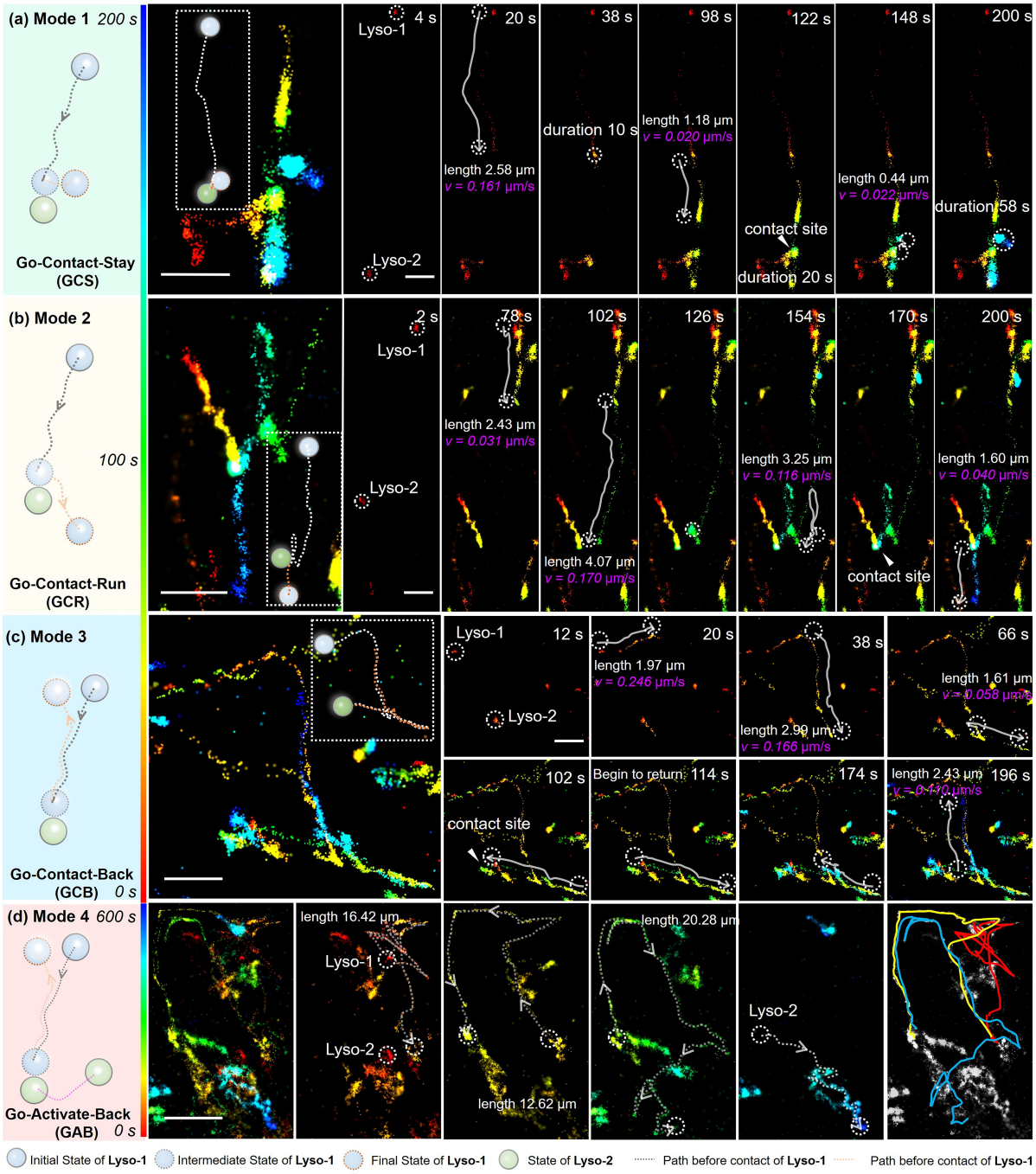

Figure 3. Long-term SMLM imaging of Lyso–Lyso contact modes in live HeLa cells. a) "Go-Contact-Stay" (GCS), scale bar: 0.5 μm. b) "Go-Contact-Run" (GCR), scale bar: 0.5 μm. c) "Go-Contact-Back" (GCB), scale bar: 1.0 μm. d) "Go-Activate-Back" (GAB), scale bar: 2.0 μm.

started to move back and forth in a localized area until 153 seconds. In another scenario, Lyso-1 shown in Figure 2m underwent a triangular reentry quickly, where the two adjacent routes just covered a distance of 82.6 nm. From 185 seconds, Lyso-3 entered the area where Lyso-1 and Lyso-2 were located, and from this time until 292 seconds, Lyso-1 and Lyso-2 were stationary, while Lyso-3 had been moving back and forth in a straight line at high speed (0.252–0.260 $\mu m\,s^{-1}$). Lyso-3 came into contact with Lyso-2 at 209seconds and then quickly returned along the original route. The distance resolution of the two routes in Figure 2n showed that the trajectories of Lyso-3 before and after contact with Lyso-2 were completely coincident. We carefully studied the movement trajectories of multiple lysosomes in different cells, as shown in Figure 2o and S27–31, and found that their movement paths were diverse and complex, and all contained deflection and reentrant motion nodes. Importantly, our new self-blinking fluorophore, **LysoSR-549**, permitted 3D long-term SMLM super-resolu-

tion imaging of lysosomal dynamics and revealed the diversity of their movements at the nanoscale (Figure S27).

Pervasive interactions between lysosomes have also been observed with long-term nanoscopy. Based on our data, we obtained four representative interaction modes, namely "Go-Contact-Stay" (GCS), "Go-Contact-Run" (GCR), "Go-Contact-Back" (GCB), and "Go-Active-Back" (GAB), respectively, according to the change of motion trajectories before and after contact. In GCS (Figure 3a, S28 Movie 4), Lyso-1 started to move towards Lyso-2 with an initial speed of 0.161 $\mu m s^{-1}$, and gradually slowed down to 0.020 $\mu m s^{-1}$ until it reached a stationary state upon contact with Lyso-2 at 122 seconds. In GCR (Figure 3b, S29 Movie 5), Lyso-1 continued to move forward after contact with Lyso-2, while Lyso-2 stayed in place. During this process, the movement speed of Lyso-1 was constantly changing. In both GCB and GAB (Figure 3c,d, S30, S31, Movie 6, 7), Lyso-1 returned to its original path after contact with Lyso-2. The difference was that in GAB, Lyso-2 would become "activated" upon contact and begins to move after contact. As shown in Figure 3c and Movie 6, Lyso-1 made contact with Lyso-2 at 102 s and then moved towards opposite directions at 114 s. Of noteworthy, the forward path at 38–102 s coincides with the return path at 114–196 s. In GAB, we observed the longest motion trajectory, that is, 50 microns of continuous movement for 600 seconds (Figure 3d, Movie 7).

The analysis of the dynamics and chemical composition of the lysosomes can be used to diagnose lysosomal diseases. We analyzed intracellular lysosomes under different external stimuli and found that the size, number, distribution, dynamics, and intraluminal pH of lysosomes were significantly different under different conditions (Figure 4). From Figure 2a and Figure 4a–f, lysosomes exhibited completely different distributions and dynamics under different conditions, namely normal, alkaline, acidic, starvation, apoptosis, and cell division. In alkaline, starved, and CCCP treated cells, the lysosomes were found to be more concentrated around the nucleus (Figure 4a, b, d, e); in acidic conditions and prior cell division, the lysosomes were more dispersed along the periphery of the cell (Figure 4c, f). For healthy cells, the size of perinuclear lysosomes (139 ± 42 nm) was much larger than peripheral lysosomes (124 ± 26 nm) due to the frequent fusion near microtubule organizing centers (MTOC) (Figure S32). However, the size of lysosomes in the five conditions was significantly changed compared with that in healthy cells ($p < 0.0001$; here p is the parameter used to measure the difference in statistics) (Figure 4g, S33–S38). Among them, the size of cells treated with alkaline solutions increased significantly (187 ± 52 nm at 4 mM NH_4Cl, 303 ± 84 nm at 10 mM NH_4Cl), and the size of lysosomes in cells treated with other conditions decreased (116 ± 26 nm for acidification; 114 ± 29 nm for starvation; 118 ± 23 nm for apoptosis). Based on the dependence of the number of photons on pH (Figure 1d, S11), we found that the lysosomal pH in cells in different conditions also changed accordingly (Figure 4h, S33–S38). In cells exposed to alkaline conditions, the number of photons per event was significantly reduced, indicating an increase in lysosomal pH. In starved and acidified cells, the number of photons per event was significantly increased, indicating a decrease in lysosomal pH, with little difference in their size. Lysosomal pH was slightly elevated in apoptotic and dividing cells. These observed changes, enabled by the photophysical properties of the probe, are expected to be useful in the characterization of lysosomal dysfunctional diseases.

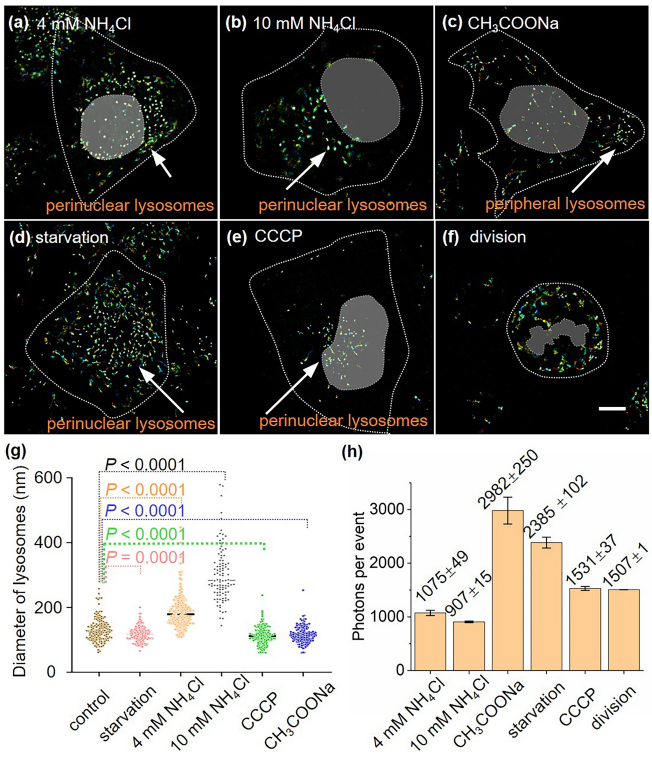

Figure 4. SMLM imaging of lysosomes in live HeLa cells with 4 mM NH_4Cl (a), 10 mM NH_4Cl (b), CH_3COONa (c), starvation (d) and CCCP (e). f) SMLM imaging of lysosomes in dividing cells. Scale bar: 5.0 μm. g) Statistics of the diameters of lysosomes in live cells. h) Photons per switching event of (a–f).

In conclusion, we have developed **LysoSR-549** as a self-blinking fluorophore for SMLM imaging of lysosomes by the introduction of pyridine to regulate the ring-opening reaction of rhodamine spirolactam at lysosomal pH. **LysoSR-549** exhibited stable and reproducible switching performance, pH dependence, and buffering capacity in lysosomes, enabling long-term stable imaging of lysosomes at the nanoscale. **LysoSR-549** resolves the dynamics of whole-cell lysosomes and changes in luminal pH under different conditions and is expected to be useful for the analysis of lysosomal functions and pathological diagnosis.

Acknowledgements

This work is supported by the National Natural Science Foundation of China (22078314, 21878286, 21908216) and the Ministry of Education, Singapore (MOE-MOE-T2EP10120-0007).

Conflict of Interest

The authors declare no conflict of interest.

Data Availability Statement

The data that support the findings of this study are available in the supplementary material of this article.

Keywords: Long-Term Nanoscopy · Lysosomes · Organelle Dynamics · Rhodamine Spirolactam · Self-Blinking

[1] a) C. de Duve, *Nat. Cell Biol.* **2005**, *7*, 847–849; b) R. E. Lawrence, R. Zoncu, *Nat. Cell Biol.* **2019**, *21*, 133–142.
[2] A. Ballabio, J. S. Bonifacino, *Nat. Rev. Mol. Cell Biol.* **2020**, *21*, 101–118.
[3] D. Chen, W. Liu, J. Zimmerman, W. A. Pastor, R. Kim, L. Hosohama, J. Ho, M. Aslanyan, J. J. Gell, S. E. Jacobsen, A. T. Clark, *Cell Rep.* **2018**, *25*, 3591–3602.
[4] R. Matteoni, T. E. Kreis, *J. Cell Biol.* **1987**, *105*, 1253–1265.
[5] a) J. Heuser, *J. Cell Biol.* **1989**, *108*, 855–864; b) B. Suresh, A. Saminathan, K. Chakraborty, M. Zajac, C. Cui, L. Becker, Y. Krishnan, *Proc. Natl. Acad. Sci. USA* **2021**, *118*, e2113174118.
[6] K. Leung, K. Chakraborty, A. Saminathan, Y. Krishnan, *Nat. Nanotechnol.* **2019**, *14*, 176–183.
[7] J. Chen, C. Wang, W. Liu, Q. Qiao, H. Qi, W. Zhou, N. Xu, J. Li, H. Piao, D. Tan, X. Liu, Z. Xu, *Angew. Chem. Int. Ed.* **2021**, *60*, 25104–25113; *Angew. Chem.* **2021**, *133*, 25308–25317.
[8] Z. Ye, W. Yang, C. Wang, Y. Zheng, W. Chi, X. Liu, Z. Huang, X. Li, Y. Xiao, *J. Am. Chem. Soc.* **2019**, *141*, 14491–14495.
[9] S.-N. Uno, M. Kamiya, T. Yoshihara, K. Sugawara, K. Okabe, M. C. Tarhan, H. Fujita, T. Funatsu, Y. Okada, S. Tobita, Y. Urano, *Nat. Chem.* **2014**, *6*, 681–689.
[10] H. Takakura, Y. Zhang, R. S. Erdmann, A. D. Thompson, Y. Lin, B. McNellis, F. Rivera-Molina, S.-N. Uno, M. Kamiya, Y. Urano, J. E. Rothman, J. Bewersdorf, A. Schepartz, D. Toomre, *Nat. Biotechnol.* **2017**, *35*, 773–780.
[11] W. Chi, Q. Qiao, C. Wang, J. Zheng, W. Zhou, N. Xu, X. Wu, X. Jiang, D. Tan, Z. Xu, X. Liu, *Angew. Chem. Int. Ed.* **2020**, *59*, 20215–20223; *Angew. Chem.* **2020**, *132*, 20390–20398.

Manuscript received: February 23, 2022
Accepted manuscript online: March 9, 2022
Version of record online: ■■, ■■

Communications

Fluorescent Probe

Q. Qiao, W. Liu, J. Chen, X. Wu, F. Deng, X. Fang, N. Xu, W. Zhou, S. Wu, W. Yin, X. Liu, Z. Xu* e202202961

An Acid-Regulated Self-Blinking Fluorescent Probe for Resolving Whole-Cell Lysosomes with Long-Term Nanoscopy

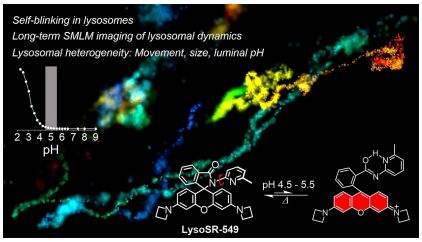

LysoSR-549 as a self-blinking fluorophore for SMLM imaging of lysosomes is reported. It enables simultaneous dynamic and pH recognition of all lysosomes in the entire cell at the single-lysosome-resolved level, which allowed to resolve whole-cell lysosome subpopulations based on lysosome distribution, size, luminal pH, movement trajectories and interactions between lysosomes.